



**HAL**  
open science

## Simulation of Single Particle Displacement Damage in Silicon – Part III: First Principles Characterization of Defect Properties

Antoine Jay, Anne Hémercyck, Nicolas Richard, Layla Martin-Samos, Melanie Raine, Alexandre Le Roch, Normand Mousseau, Vincent Goiffon, Philippe Paillet, Marc Gaillardin, et al.

### ► To cite this version:

Antoine Jay, Anne Hémercyck, Nicolas Richard, Layla Martin-Samos, Melanie Raine, et al.. Simulation of Single Particle Displacement Damage in Silicon – Part III: First Principles Characterization of Defect Properties. IEEE Nuclear and Space Radiation Effects Conference, Jul 2017, New Orleans, United States. hal-01685635

**HAL Id: hal-01685635**

**<https://hal.science/hal-01685635>**

Submitted on 16 Jan 2018

**HAL** is a multi-disciplinary open access archive for the deposit and dissemination of scientific research documents, whether they are published or not. The documents may come from teaching and research institutions in France or abroad, or from public or private research centers.

L'archive ouverte pluridisciplinaire **HAL**, est destinée au dépôt et à la diffusion de documents scientifiques de niveau recherche, publiés ou non, émanant des établissements d'enseignement et de recherche français ou étrangers, des laboratoires publics ou privés.

# Simulation of Single Particle Displacement Damage in Silicon – Part III: First Principles Characterization of Defect Properties

Antoine Jay, *Member IEEE*, Anne Hémercyck, Nicolas Richard, *Member IEEE*, Layla Martin-Samos, Mélanie Raine, *Member IEEE*, Alexandre Le Roch, Normand Mousseau, Vincent Goiffon, *Member IEEE*, Philippe Paillet, *Senior Member IEEE*, Marc Gaillardin, *Member IEEE*, Pierre Magnan, *Member, IEEE*

**Abstract** – A first principles study of the defects generated by displacement cascades from previous Molecular Dynamics (MD) and kinetic Activation Relaxation Technique (k-ART) simulations [1,2] in bulk silicon is performed. Structural, energy and migration properties are evaluated using standard Density Functional Theory (DFT) calculations. Electronic properties are obtained through the application of the Many Body Perturbation Theory (MBPT) in the  $G_0W_0$  approximation. Electronic states introduced in the electronic structure of bulk silicon are then given. The obtained properties allow to get a first reconstruction of the signal generated by each defects. Here we particular focus on two types defects, the di-vacancy and the tri-interstitial, and we discuss their major contribution to Dark Current (DC) and to Dark Current Random Telegraph Signal (DC-RTS) respectively.

**Index Terms**– Silicon, Displacement Damage, First Principles Calculations, kinetic Activation Relaxation Technique, Defects, Dark current, Random Telegraph signal.

## I. INTRODUCTION

THE need for fundamental understanding of the damaged structures generated at the atomic scale by Displacement Damage (DD) is a major challenge for the community of radiation effects on micro and optoelectronics (see among others [3]). To tackle this question, a novel simulation approach based on the one proposed by Srour and Palko [3] has been presented and applied in [1] and [2]. It combines several simulation methods linked one to another as shown in Fig. 1: Monte Carlo particle-matter interaction simulation, Molecular Dynamics (MD), kinetic Monte Carlo (KMC) and first principles (FP) calculations (also called *ab initio*

calculations). Results coming from the first step and from the second and third steps are presented in [1] and [2] respectively. As detailed in [1], the main advantages of this methodology are the following: simulations start from realistic PKA (Primary Knock-on Atom) energies; large statistics of possible PKA directions are simulated resulting in a library of generated defects; the electronic stopping power is taken into account; simulation times on the order of one second are reached, giving access to direct comparison with experimental data. This last crucial point has been obtained by using a KMC method called the kinetic Activation Relaxation Technique (k-ART) [4]. This method, by overtaking the timescale limit of classical MD simulations, offers the possibility of relaxing a large library of defects and defect clusters during 1s after the initial interaction as demonstrated in [2]. The access to this long time scale has enabled to draw some first important conclusions regarding the origin of the Dark Current (DC) and Dark Current-Random Telegraph Signal (DC-RTS) measured in image sensors as discussed in [2]:

- After one second of annealing, clusters are constituted of small defects, such as bi-, tri- and quadri-vacancies and interstitials (1 to 4-V and 1 to 4-I respectively). This is due to the fact that point defects and small defect clusters tend to aggregate because of their small diffusion coefficient while large defect clusters anneal because they are mainly composed of Frenkel pairs that recombine.
- DC-RTS phenomena seem to be linked to flickering configurations, i.e. different alternating defect configurations with low barriers between them surrounded by large energy barriers.
- Calculations found that the cluster size distribution presents an exponential shape similar to the shape of the dark current (DC) distribution measured experimentally in image sensors [5].

The present paper carries on this approach by characterizing the damaged structures obtained at the end of the k-ART step using FP calculations (final step identified in red in Fig. 1). They are analyzed and compared with experimental results on image sensors. The final goal is to understand how the defect properties may be linked to the DC and DC-RTS phenomena observed in image sensors. In particular, we focus here on two “simple” defects clusters, i.e. the bi- vacancies (2V) and

A. Jay, V. Goiffon, A. Le Roch and P. Magnan are with ISAE, Université de Toulouse, 10 av. E. Belin, F-31055 Toulouse, France ([antoine.jay@isae.fr](mailto:antoine.jay@isae.fr)).

A. Hémercyck is with LAAS/CNRS, 7, av. du Col. Roche, F-31031 Toulouse, France ([anne.hemeryck@laas.fr](mailto:anne.hemeryck@laas.fr)).

N. Richard, M. Raine, P. Paillet and M. Gaillardin are with CEA, DAM, DIF, F-91297 Arpajon, France ([nicolas.richard@cea.fr](mailto:nicolas.richard@cea.fr)).

N. Mousseau is with Université de Montréal, C.P. 6128, Succursale Centre-Ville, Montréal, CA-H3C 3J7, Québec, Canada ([normand.mousseau@umontreal.ca](mailto:normand.mousseau@umontreal.ca)).

Layla Martin-Samos is with Materials Research Laboratory at University of Nova Gorica, Vipavska 11c SI-5270 Ajdovščina, Slovenia ([layla.colomer@ung.si](mailto:layla.colomer@ung.si)).

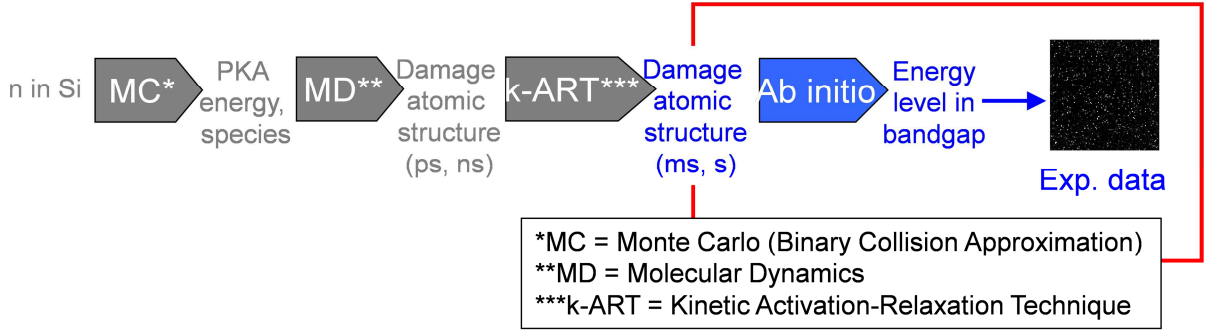


Fig.1: Schematic of the global simulation project. The steps inside the scope of this paper are identified by red squares. The Part I and Part II correspond to two previous papers [1] and [2]. Methods used are into the blue arrows. MC: Monte-Carlo. MD: Molecular Dynamics. k-ART: Kinetic Activation Relaxation Technique.

the tri-interstitial (3I), as it appears that their behavior can be correlated to DC-RTS and DC phenomena respectively.

In this paper, the details of the FP calculations are described in the first part. The results concerning the defect properties at the atomic scale are then exposed in the second part, mostly regarding their lifetimes and electronic levels in the gap. These results are then linked to the macroscopic DC and DC-RTS phenomena observed in image sensors in the last part.

## II. CALCULATIONS DETAILS

FP calculations are used to obtain the total energy and electronic properties of each simple defect configuration extracted from the k-ART simulations. To do so, these configurations are embedded within a perfect diamond-like crystalline cell of about 216 atoms (*i.e.* 216 atoms corresponding to  $3 \times 3 \times 3$  elementary cells) for the perfect crystalline diamond Si cell without defects, 215 atoms for a mono-vacancy and 217 atoms for a mono-interstitial, 214 atoms for a di-vacancy and so on). This procedure leads to computationally affordable cell sizes for FP calculations and to a large distance, of about 30 Å, between the cluster defect and its periodic images.

To relax the structures obtained from k-ART [2], DFT calculations in the Local Density Approximation (LDA) have been performed with the PWscf code from the Quantum ESPRESSO distribution [6]. Norm-conserving pseudopotentials are applied to describe electron-ion interactions. The plane waves cutoff energy is fixed at 60 Ry and the calculations are done at the  $\Gamma$  point (center of the Brillouin Zone). The cell parameters of each simulation cell is kept constant equal the ones of the perfect crystalline cell with its 216 atoms and only the atomic positions have been allowed to relax in order to obtain interatomic forces lower than  $10^{-3}$  Ry/a.u.

The obtained atomic positions and their corresponding wave functions (only with a cutoff energy of 20 Ry) are then used in one shot GW (*i.e.*  $G_0W_0$ ) calculations performed with the SaX package version 2.0 [7]. The calculation of electronic states is still a challenge nowadays as DFT, being a ground state theory, strongly underestimates the band gap in semiconductor and insulating materials [8]. However, [9] proved that even if

the unoccupied states are badly predicted in DFT, the energy difference between the top of the valence band and the occupied states is correct and does not vary with the opening of the band gap. The calculation of the relative positions in energy of the defect levels in the experimental gap with this technique is thus correct, without needing any shift in energy. In this work, we want to go further by getting the Density Of States (DOS) of the defects and their associated states in the DOS, allowing us to draw the complete picture of their chemistry. To do so, GW approximation is a well-established theoretical approach to answer to the DFT band gap failure, but they still require large computing resources. However, the SaX code has already proven its efficiency to treat large cells containing defects as for instance in silica [10,11].

Details of the  $G_0W_0$  calculations are the following: we adopted 20 Ry energy cutoff for the Fock operator, 20 Ry energy cutoff for the irreducible polarizability and the screened Coulomb potential. We included 1100 bands for the transition many-fold sampling, in the calculation of the GW Green functions. The Godby-Needs plasmon-pole model [12] was used to model the energy dependence of the dielectric matrix. The accuracy on the energies states in the band gap is about 0.10 eV.

An important characteristic of an electronic state is its degree of localization. It is quantified by means of a normalized Self-Interaction (|SI|), as discussed in [13]: the higher the value of SI, the stronger the localization (for |SI|=1, the electronic state is as delocalized as a plane-wave).

Migration pathways are used to calculate the average lifetimes  $\langle \tau \rangle$  of each defect structure using transition state theory that involves the knowledge of the surrounding saddle point that has the lowest energy barrier of migration  $E_b$ :

$$\langle \tau^{-1} \rangle = \frac{\prod_{min} \omega_i}{\prod_{saddle} \omega_j} e^{-\frac{E_b}{k_B T}} \quad (1)$$

where the product over all the phonon frequencies  $\omega$  on the studied structure  $\prod_{min} \omega_i$  is done over  $3N$  frequencies and  $3N-1$  on the saddle point,  $N$  being the number of atoms,  $k_B$  the Boltzmann constant and  $T$  the temperature. The ratio of

the phonon frequencies is taken to be  $10^{-13}$  Hertz as in most of the crystalline solids.

For the calculation of the migration pathways along the minimum energy path (MEP), the Climbing-Image Nudged Elastic Band (CI-NEB) is used to evaluate the energy barriers [14]. We used 13 intermediate images to describe the path with a high enough resolution in order to avoid missing an intermediate saddle point.

For a structure that has  $N$  possible configurations with respective energies  $E_{di}$  ( $i=1, \dots, N$ ), the probability  $P_i$  that the system is in the configuration  $i$  is a function of  $E_{di}$  and of the partition of configurations  $Z$  defined as  $Z = \sum_n e^{\frac{-E_{dn}}{k_B T}}$ :

$$P_i = \frac{e^{\frac{-E_{di}}{k_B T}}}{Z} \quad (2)$$

To calculate the average intensity  $\langle I_{dc} \rangle$  of the dark current generated by one single state in the gap of a defect with an energy  $E_{defect}$ , the Shockley-Read-Hall theory is used [15,16]:

$$\langle I_{dc} \rangle \propto A e^{\frac{-E_a}{k_B T}} \quad (3)$$

where the pre-factor  $A$  is a function of hole and electron capture cross sections, their thermal velocity and their population. The pre-factor  $A$  is proportional to  $T^2$  and estimated to be  $\ln(A) \approx 36$  at 300 K in our studied case, from the experimental value of the di-vacancy given in [5,17,18]. The term  $E_a$  is commonly named the activation energy needed for one electron to go from the valence band to the conduction band.

The estimation of this activation energy depends of the number of electronic states in the band gap. A state in the band gap becomes a bridge for the electrons to travel from the valence band to the conduction band. When only one state with the associated energy  $E_t$  exists in the band gap, the activation energy  $E_a$  needed to thermally activate the electrons is:

$$E_a = \max(E_t - E_v; E_c - E_t) \quad (4)$$

where  $E_v$  and  $E_c$  are the energies corresponding to the top of the valence band and the bottom of the conduction band respectively. However, when several states (for instance  $E_{t1}$  and  $E_{t2}$ ) are into the gap the electrons can sometimes use a multiple-steps bridge such as  $E_v \rightarrow E_{t1} \rightarrow E_{t2} \rightarrow E_c$ . This multiple bridge pathway can occur only if the wave functions  $|\phi_{t1}\rangle$  and  $|\phi_{t2}\rangle$  of the two states  $t1$  and  $t2$  overlap. The activation energy is then:

$$E_a = \min[\max_j(E_{j+1} - E_j); (\max_i(E_i - E_v; E_c - E_i))] \quad (5)$$

where  $i$  covers all the non-overlapping states, and  $j$  covers all the overlapping states. The dark current intensity is then calculated as in [19].

The formation energy  $E_f$  of a defect is the energy that the system has to give to create a defect. It is defined with respect to the total energy  $E_{216}$  of the pure silicon supercell as a function of the number of atoms  $n_a$  that contains the supercell and  $E_d$  the energy of the defective supercell as:

$$E_f = - \left[ E_{216} \left( \frac{n_a}{216} \right) - E_d \right] \quad (6)$$

### III. RESULTS

#### General trends

As explained in [2], a silicon PKA in bulk silicon at 300 K generates a displacement cascade which finally results in amorphous clusters that are mainly composed of small simple defects, namely 2V, 3V, 4V and 3I, 4I. The fundamental understanding of the dynamic behavior and electronic properties of these resulting simple defects can provide a good insight of the macroscopic observations on DC and DC-RTS.

Among all the simple defects, we choose to focus on two meaningful defects playing an important role in the response of silicon to DD: the di-vacancy (2V) and the tri-interstitial (3I) defects. These defects well depict the typical behaviors of DC-RTS and DC signals respectively. In fact, they both have different configurations with lifetimes that vary from micro-second to years and also possess zero to three electronic levels in the band gap. A full review paper gathering the details on all simple defects in bulk silicon will be published in a near future.

To understand the origin of the DC and the DC-RTS using FP calculations, we focus our study on the possible configurations that can have each defect, the corresponding migration barrier to travel between such configurations, their lifetimes, and the corresponding electronic levels that appear in the band gap.

For details, for a given defect, the configuration with the lowest formation energy (the ground state) is the most stable and consequently is the one that is mainly observed experimentally. But several other stable or metastable states can also exist, that can differ from the ground state by small structural changes (interatomic distances) or can be topologically different in terms of close neighborhood.

The diffusion barrier gives information about the possibility to observe the defects experimentally. Indeed, the defects that can diffuse at the experimental temperature are not observed because they tend to agglomerate to form bigger defect clusters and/or they are trapped at the interfaces. Notably, among all the simple defects, the 1V, 1I and 2I possess energy barrier that are small enough to diffuse at 300 K (0.50, 0.50 and 0.50 eV respectively) whereas the 2V, 3V, 4V and 3I, 4I exhibit migration barrier higher than 0.50 eV, that are large enough to keep these defects into the silicon bulk at room temperature. The diffusion barrier is thus calculated for each defect. Note that the diffusion coefficient depends on the temperature so that the observation time is strongly correlated to the operation temperature.

The lifetime associated to each configuration that can be taken by a defect gives information about the kind of DC generation that is created by the defect, i.e., noised DC, DC-RTS or constant DC. This depends on the experimental integration time, i.e. the duration of the accumulation of the electrons before counting them, and acquisition time (duration of the total measurement). Indeed, a defect generates a noised DC if the lifetimes of its configurations are lower than the integration time: several changes in configurations can occur during the integration time and only an average of all the generations' rates is counted, producing the noise. A defect generates DC-RTS if the lifetimes of its configurations are higher than the integration time and lower than the acquisition

time: the DC signal is constant during several periods of integrations and brutally varies when the configuration changes. Finally, a defect generates a constant DC if the lifetimes of its configurations are higher than the acquisition time: no change of configuration occurs during all the experiment. The average lifetime is a constant for a given temperature, but the kind of generation rate that is observed depends on the experimental conditions. As all the defects exist in several stable and metastable atomic configurations, they are all able to generate the three kinds of DC only measurable by changing both the integration and acquisition times.

Note that for a same defect, lifetimes can be very different. Indeed, two main trends are observed in the energy barriers required to switch from one configuration to another for the same defects. On one hand, the configurations that are topologically different are separated by energy barriers higher than  $\sim 0.40$  eV. On the other hand, the configurations that differ only by a change in their atomic distances which conserve their neighboring topology are separated by lower energy barriers.

The energy levels are the last information that is used in our study. It informs on the intensity of the generated DC. Concerning the electronic states, the same trends are observed. Configurations with the same topology exhibit very similar DOS, whereas configurations with different topologies have different DOS. The number of states in the band gap is difficult to predict and varies between zero and four in the studied defects 2V and 3I.

#### The di-vacancy defect

The di-vacancy has been widely detected in CMOS after irradiation [20] and plays a crucial role as a DC generation center. In our calculations, we observe that the di-vacancy owns a high number of metastable configurations. The most stable ones are shown in Fig. 2 and are classified from the lowest to the highest total energy: two vacancies as first neighbor (2Va), as second neighbor (2Vb), and as third neighbor (2Vc). For the 2Va configuration, two configurations exist, named 2Va<sub>2</sub> and 2Va<sub>4</sub> (Fig 2.a and 2.b), 2Va<sub>2</sub> being the most stable one. Contrary to the 2Va, 2Vb and 2Vc configurations that have a different topology, 2Va<sub>2</sub> and 2Va<sub>4</sub> are only distinguishable by their different interatomic distances. In fact, due to the local reconstruction, a weak electronic bond is also sometimes formed between two Si atoms when the interatomic distance is lower than 3.0 Å.

The Minimum Energy Path (MEP) for the diffusion of the di-vacancy from its ground state 2Va<sub>2</sub> to a neighbor 2Va<sub>2</sub> occurs through the 2Vb or 2Vc configuration. This diffusion needs the crossing of a 1.11 eV energy barrier as shown in Figure 3 for Va<sub>2</sub>, coherent with the experimental observation [21], so that no diffusion can be observed at 300 K. The 2Vb configuration is a highly metastable state that rapidly tends to stabilize in the ground state 2Va<sub>2</sub>.

The resulting lifetimes, the occupation probabilities and the diffusion barriers for the 2V configurations are summarized in Table I.

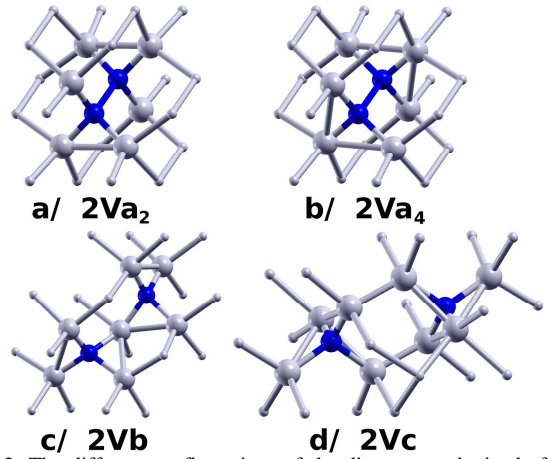


Fig. 2: The different configurations of the di-vacancy obtained after k-ART simulations and relaxed and characterized using FP calculations. a/ 2Va<sub>2</sub>, b/ 2Va<sub>4</sub>, c/ 2Vb d/2Vc. Grey balls: Silicon atoms. Big grey balls: first neighbor silicon atoms of a vacancy. Blue balls: crystalline sites without any atoms, i.e., vacancies.

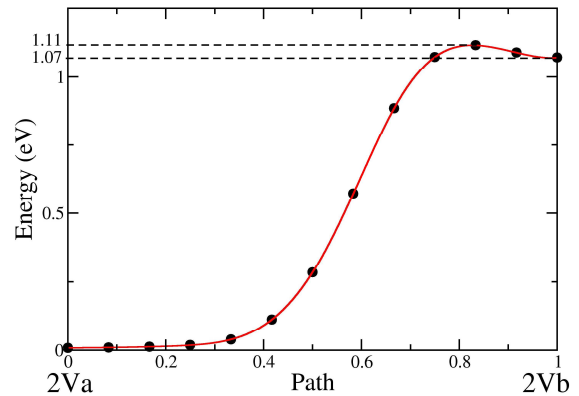


Fig. 3. Migration path between the 2Va<sub>2</sub> and the 2Vb configurations. The energy barrier 2Va<sub>2</sub>→2Vb<sub>2</sub> is 1.11 eV whereas the energy barrier 2Vb<sub>2</sub>→2Va<sub>2</sub> is 0.04 eV.

The occupation probabilities of the 2Vb and 2Vc configurations are very small, so that they would not be observed experimentally. Nevertheless 2Vb and 2Vc are metastable “transition” states that are reached during the diffusion process of the di-vacancy.

TABLE I  
UPPER PART: THE DIFFUSION BARRIER IN EV FROM ONE TO ANOTHER 2V CONFIGURATIONS. LOWER PART, FOR EACH 2V CONFIGURATION: THE FORMATION ENERGY E<sub>f</sub> IN EV/AT. THE TOTAL ENERGY WITH RESPECT TO THE GROUND STATE 2Va<sub>2</sub> EV, THE AVERAGE LIFE TIME <τ> AT 300 K IN S AND THE OCCUPATION PROBABILITY P.

From/to	2Va <sub>2</sub>	2Va <sub>4</sub>	2Vb	2Vc
2Va <sub>2</sub>	-	0.004	0.04	0.61
2Va <sub>4</sub>	0.004	-	0.04	0.61
2Vb	1.11	1.11	-	0.06
2Vc	1.92	1.92	0.36	-
	2Va <sub>2</sub>	2Va <sub>4</sub>	2Vb	2Vc
E <sub>f</sub>	4.92	4.92	5.99	6.28
ΔE	0	0	1.07	1.36
<τ>	10 <sup>-13</sup>	10 <sup>-13</sup>	10 <sup>-13</sup>	10 <sup>-12</sup>
P	0.50	0.50	10 <sup>-19</sup>	10 <sup>-24</sup>

On the contrary, the two 2Va configurations are the ones with the largest occupation probabilities. Because of their equal formation energies, these two probabilities are equivalent. However, the lifetimes of these two 2Va configurations are very small (less than one μs) because of

the small energy barrier (0.004 eV) that separates them, so that these two structures pass from one state to the other billion times per seconds at 300 K. The  $2V_a$  system is thus trapped in a quasi-permanent oscillation between the two configurations  $2V_{a_2}$  and  $2V_{a_4}$ , whereas the high energy barriers (1.11 eV) required to separate the two vacancies can not be overcome at 300 K.

The DOS is given in Fig. 4 for the  $2V_{a_2}$  and  $2V_{a_4}$  configurations in GW approximations. The GW approximation gives a band gap of 1.06 eV, with only 5% of error compared to experimental value equal to 1.12 eV [22] vs. 50% for DFT (not shown here).

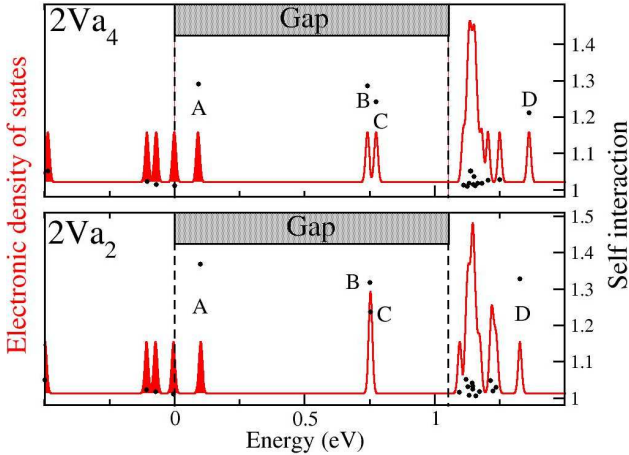


Fig. 4. DOS calculated within GW approximation for the most observed configurations of di-vacancy defect: the  $2V_{a_4}$  (top) and  $2V_{a_2}$  (bottom). Letters are here to mark the defect energy levels. The states occupied at 0 K are filled.

Three electronic levels have been observed experimentally, supposed in one of the most probable configurations ( $2V_{a_2}$  or  $2V_{a_4}$ ):

- by Electronic Paramagnetic Resonance (EPR):  
Ec-0.23 eV (charged -) [21]
- by Infrared spectroscopy (IR):  
Ec-0.39 eV (charged 0) [21]
- by Deep-level transient spectroscopy (DLTS):  
Ev+0.21 eV (charged +) [21,22]

where Ev and Ec are the top of the valence band and the bottom of the conduction band, respectively. In [21] and [22], authors explain that Ev+0.21 eV is a holes acceptor state whereas Ec-0.23 eV and Ec-0.39 eV are electrons acceptors states. In our results, for  $2V_{a_4}$  we find the holes acceptor at Ev+0.09 eV and the two electrons acceptor states are located at Ec-0.29 eV and Ec-0.32 eV.

The |SI| allows to distinguish the states induced by the defect. As shown in Fig. 4, the  $2V_{a_2}$  configuration generates four main states, namely A, B, C and D. Among them, only the states A, B, and C are into the band gap and only the state A is filled at 0 K, in good agreement with the experimental observations [19,21]. All these states can serve as “bridges” for the electrons to travel from the valence band to the conduction band. To evaluate the activation energy of this defect using Eq. 5, one should first evaluate the overlapping integral between these defect states. For the three states A, B and C in the band gap, the presence probability is drawn in Fig. 5. It shows that no overlapping occurs between the state A and the state B nor between the state B and the state C because the electrons are located on different atoms. On the contrary, a drastic overlapping occurs between the state A and the state C,

because they both form a dangling bond on the same atom and in the same direction. In the specific case of  $2V_{a_2}$ , the calculated activation energy is then determined between the energy levels of the two states A and C:  $|0.75-0.10|=0.65$  eV.

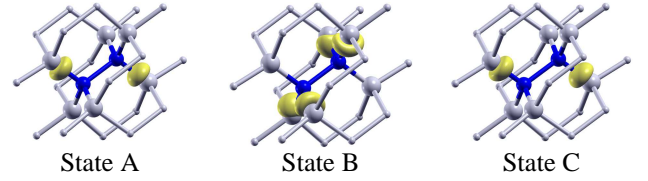


Fig. 5. Electronic wave functions square of the three electronic states A, B, C in the band gap of bulk silicon due to  $2V_{a_2}$  configuration. The yellow surface represents the isovalue for a probability to find the electron in this region equal 50%.

For all  $2V$  configurations, the energy levels into the band gap are summarized in Tab. II, with the corresponding estimated generation rate. As the two  $2V_a$  configurations have the same topology, their respective DOS exhibits slight differences, with the same number of defect states and differences in the total energy smaller than 0.02 eV. However, this is enough to slightly change the activation energy and then highly change the generation rate, because of its exponential form (see Table II).

In the case of the  $2V_b$  and  $2V_c$  configurations, different DOS with a different number of states due to their different topology are obtained. The overlapping integral between the states of the  $2V_b$  and  $2V_c$  structures are null, so that the Eq. 4 is used to evaluate the activation energy.

TABLE II  
FOR EACH CONFIGURATION OF THE DI-VACANCY DEFECT, ENERGY LEVELS INTRODUCED IN THE BAND GAP IN EV, ACTIVATION ENERGY  $E_a$  IN EV AND ITS GENERATION RATES R IN E/S BY USING  $\ln(A)=36$ .

Conf.	Energy levels	$E_a$	R
$2V_{a_2}$	0.10; 0.75; 0.75	0.65	150
$2V_{a_4}$	0.09; 0.74; 0.77	0.64	141
$2V_b$	0.91; 1.01	0.91	2
$2V_c$	0.80; 0.84	0.80	4

### The tri-interstitial defect

The same approach is conducted for the tri-interstitial defect.

The tri-interstitial exists in several configurations [23], where the two most stable are the  $3I_{\text{block}}$  and the  $3I_{\text{tetra}}$  ones shown in Fig. 6. The other configurations are much higher in total energy or correspond to the di-interstitial surrounded by another interstitial.

The MEP for the diffusion of the tri-interstitial from its ground state  $3V_{\text{tetra}}$  to a neighbor  $3V_{\text{tetra}}$  needs the crossing of a 0.45 eV barrier, whereas this barrier is 2.59 eV for the diffusion from a  $3V_{\text{block}}$  configuration to a  $3V_{\text{block}}$  configuration. For this reason, during annealing all the  $3V_{\text{tetra}}$  configurations diffuse, whereas the  $3V_{\text{block}}$  does not.

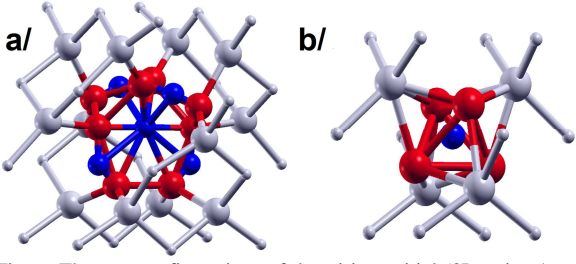


Fig. 6. The two configurations of the tri-interstitial ( $3I_{\text{block}}$  in a/ and  $3I_{\text{tetra}}$  in b/) obtained after k-ART simulations and relaxed and characterized using FP calculations. Grey balls: Silicon atoms. Big grey balls: silicon atoms in first neighbor of a vacancy. Blue balls: crystalline sites without atoms, i.e., vacancies. Red ball: interstitial silicon atoms.

Their average lifetime and occupation probability are given Tab. III. These two structures have quite the same formation energy ( $\Delta E=0.02$  eV), so that their occupation probabilities are of the same order of magnitude. The energy barrier that separates them is very large ( $> 2$  eV), which means that their configuration change from one to another cannot be observed experimentally during reasonable times.

TABLE III.

FOR EACH CONFIGURATION OF THE TRI-INTERSTITIAL, ITS FORMATION ENERGY  $E_F$  (EV/AT.), ITS ENERGY WITH RESPECT TO THE GROUND STATE (EV), ITS AVERAGE LIFE TIME  $\langle T \rangle$  AT 300 K (S), ITS AVERAGE OCCUPATION  $\langle \text{OCC.} \rangle$  AMONG ALL THE CONFIGURATIONS (%) AND ITS MINIMUM ENERGY NEEDED TO GO FROM ONE CONFIGURATION TO ANOTHER. ALL THE VALUES ARE IN EV.

From/to	$3I_{\text{tetra}}$	$3I_{\text{block}}$
$3I_{\text{tetra}}$	-	2.60
$3I_{\text{block}}$	2.62	-
$E_f$	5.39	5.41
$\Delta E$	0	0.02
$\langle T \rangle$	$10^{31}$	$10^{31}$
P	0.68	0.32

The energy levels and generation rates of the two configurations are given Tab. IV. The configuration  $3I_{\text{block}}$  does not create energy levels in the band gap. Hence its generation rate  $R$  is null. On the contrary, the configuration  $3I_{\text{tetra}}$  has a generation rate, which means that those two structures can be easily distinguished using at  $E_a$  or  $R$ .

TABLE IV

FOR EACH CONFIGURATION OF THE TRI-INTERSTITIAL DEFECT, ENERGY LEVELS INTRODUCED IN THE GAP (EV), ACTIVATION ENERGY  $E_a$  (EV) AND ITS GENERATION RATES  $R$  (E-/S) BY TAKING  $\text{LN}(A)=36$ .

Conf.	Energy levels	$E_a$	R
$3I_{\text{block}}$	-	1.06	0
$3I_{\text{tetra}}$	0.92	0.92	2

#### IV. DISCUSSION

##### Average DC, Constant DC or DC-RTS?

In this section, we use the FP results for the di-vacancy and tri-interstitial defects to investigate if their presence in a CMOS image sensor generates or not a dark current, and if this dark current is a RTS.

Even if both 3I and 2V defects exist as several configurations and exhibit electronic levels into the band

gap, they do not generate the same DC. Actually, the main difference between the 3I and the 2V defects comes from their lifetimes due to stability of their configurations.

In the case of the 3I, each configuration is trapped in a deep potential energy well giving to it a great stability. Their resulting lifetimes are higher than one year so that a configuration can hardly change during an experimental observation. Moreover, the  $3I_{\text{block}}$  configuration does not have any states in its band gap (Tab. III) and is then not a generation center and no DC is observed. On the contrary, the  $3I_{\text{tetra}}$  configuration has one state into its band gap and is a generation center. Its resulting signal is then a permanent DC.

In the case of the 2V, a high number of transitions between  $2Va_2$  and  $2Va_4$  occurs during a same integration time (several milliseconds), so that experimentally, the integration time is generally too high to observe them separately. Hence, during an acquisition, the observed generation rate is an average of the rates of each configuration.

Nevertheless, through temperature modifications, the lifetime of each structure varies so that a DC-RTS can be observed for the 3I by increasing the temperature, and for 2V, by decreasing the temperature.

##### Electronic hopping transport between defect centers

One of the key questions concerning charge generation in thermally activated clusters is the possibility of observing Inter-Center Charge Transfer (ICCT) between spatially separated defects, i.e. that electrons hop through different localized electronic states in the band gap. For such a process, two conditions are required:

- as for standard excitation with one single state, the thermal energy  $k_B T$  must be higher than the energy difference between the two states,
- the overlap between the wave functions of the two states involved in the hopping (initial and final states) has to be non-negligible.

In the case of the  $2Va_2$ , the electronic hopping can occur thanks to the overlapping, as already discussed above and shown in Fig. 5.

In the case of a cluster made of several defects, to favor the overlapping probability and then the ICCT, the inter-defect distance in the cluster must be as small as possible, and the complexity of the defect must be as high as possible. Indeed, complex defects lead to a higher number of states than the simple ones, and to wave functions with a higher spatial expansion, because of the large number of broken and new bonds. For illustration, we plot the wave function of the  $3I_{\text{tetra}}$  state (located at 0.92 eV) in Fig. 7, which highlights a more extended wave function than the 2V presented in Fig. 5.

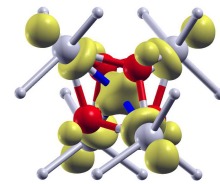


Fig. 7. Example of expansions of the wave functions that are larger than the defect: the tri-interstitial  $3I_{\text{tetra}}$  state in the band gap. The yellow surface represents the isovalue for a probability to find the electron in this region equal 50%.

Complex defects also induce more extended elastic distortions. These elastic distortions are notably responsible of the band gap narrowing by the addition of states around the valence and the conduction band. These states can have a large spatial expansion (about 15 Å) and can then overlap with more distant surrounding defects. Therefore, the probability of having ICCT into a cluster of defects increases with the number of defects it contains. Moreover, the intensity of the generated DC is highly increased when ICCT is possible. Hence, the few big clusters obtained after an irradiation generate more dark current than the numerous small clusters. This result is consistent with the observation that the histogram of the measured dark current intensity has the same exponential shape [18] than the one of the histogram of the calculated clusters' size [2].

## V. CONCLUSION

In order to describe the displacement damage in silicon, we carry on our original simulation approach by characterizing the defect structures coming from *k*-ART calculations using FP calculations. Here we focus on the di-vacancy and tri-interstitial defects and FP calculated properties of others defects (1V, 3V, 4V and 1I, 2I, 4I) will be the subject of a future review publication. We evaluate their atomic structures and we calculate their formation energy, their occupation probability and their lifetimes using NEB. By using GW to calculate their DOS, we show that the states created by each configuration of a same

## REFERENCES

- 
- [1] M. Raine, A. Jay, N. Richard, V. Goiffon, S. Girard, M. Gaillardin and P. Paillet, "Simulation of Single Particle Displacement Damage in Silicon – Part I: Global Approach and Primary Interaction Simulation," *IEEE Trans. Nuc. Sci.*, vol. 64, pp. 133, 2017.
- [2] A. Jay, M. Raine, N. Richard, N. Mousseau, V. Goiffon, A. Hémerlyck, and P. Magnan, "Simulation of Single Particle Displacement Damage in Silicon–Part II: Generation and Long-Time Relaxation of Damage Structure," *IEEE Trans. Nuc. Sci.*, vol. 64, pp. 141, 2017.
- [3] J. R. Srour and J. W. Palko, "Displacement Damage Effects in Irradiated Semiconductor Devices," *IEEE Trans. Nuc.Sci.*, vol. 60, pp. 1740, 2013.
- [4] L. K. Béland, P. Brommer, F. El-Mellouhi, J.-F. Joly and Normand Mousseau, "Kinetic activation-relaxation technique," *Phys. Rev. E*, vol. 84, pp. 046704, 2011.
- [5] J.M. Belloir, V. Goiffon, C. Virmontois, P. Paillet, M. raine, R. Molina, C. Durmez, O. Gilard and P. Magnan, "Dark Current Spectroscopy in neutron, proton and ion irradiated CMOS Image Sensors: from Point Defects to Clusters," *IEEE Trans. Nuc. Sci.*, vol. 64, pp. 27, 2017.
- [6] P. Giannozzi *et al.*, "QUANTUM ESPRESSO: a modular and open-source software project for quantum simulations of materials," *J. Phys. Condens. Matter*, vol. 21, pp. 395502, 2009.
- [7] L. Martin-Samos and G. Bussi, "SaX: An open source package for electronic-structure and optical-properties calculations in the GW approximation," *Comput. Phys. Commun.*, vol. 180, pp. 141, 2009.
- [8] See among others articles: M. van Schilfgaarde, T. Kotani, and S. Faleev, "Quasiparticle Self-Consistent GW Theory," *Phys. Rev. Lett.*, vol. 96, pp. 226402, 2006.
- [9] P. A. Schultz, "Theory of Defect Levels and the "Band Gap Problem" in Silicon," *Phys. Rev. Lett.*, vol 96, pp. 246401, 2006.

defect in the band gap of silicon can lead to different dark current values. These configurations with different properties can lead to DC or DC-RTS as a function of experimental integration time. A discussion has been made on the spatial expansion of the wave functions associated to the defect states to evaluate the inter-center charge transfer possibility. This paper demonstrates the ability of our simulation approach to obtain results that can be discussed and compared to experimental characterizations. Of course, reality is much more complex: for instance, dopants and impurities are present in silicon whereas we only treat pure silicon, and in CMOS defects could be submitted to an electrical field. Another key parameters used in the SRH theory that have not been calculated for the moment are the electronic and holes cross sections. They vary of several orders of magnitude ( $10^{-13}$  to  $10^{-16}$  cm<sup>2</sup> [20]) for a given defect, highly changing the resulting generation rate. We plan to address these questions in future studies.

## ACKNOWLEDGMENT

The authors would like to thank S. Girard, J.M. Belloir, C. Virmontois and C. Durmez for fruitful discussions. The computer simulations were performed using HPC resources from GENCI-CCRT (Grant A0010907474) and from CALMIP (Grant P1555).

- 
- [10] N. Richard, L. Martin-Samos, S. Girard, A. Ruini, A. Boukenter, Y. Ouerdane and J.-P. Meunier, "Oxygen Deficient Centers in silica: optical properties within many-body perturbation theory," *J. Phys.: Condens. Matter*, vol. 25, pp 335502, 2013.
- [11] B. Winkler, L. Martin-Samos, N. Richard, L. Giacomazzi, A. Alessi, S. Girard, A. Boukenter, Y. Ouerdane, and M. Valant, "Correlations between Structural and Optical Properties of Peroxy Bridges from First Principles," *J. Phys. Chem. C*, vol. 121 pp. 4002–4010, 2017.
- [12] R.W. Godby and R. J. Needs, "Metal-insulator transition in Kohn-Sham theory and quasiparticle theory," *Phys. Rev. Lett.* vol. 62 pp. 1169, 1989.
- [13] L. Martin-Samos, G. Bussi, A. Ruini, E. Molinari and M.J. Caldas, "Unraveling effects of disorder on the electronic structure of SiO<sub>2</sub> from first principles," *Phys. Rev. B*, vol. 81, pp. 081202(R), 2010.
- [14] G. Henkelman, B. P. Uberuaga, H. Jonsson, "A climbing image nudged elastic band method for finding saddle points and minimum energy paths," *J. of Chem. Phys.*, vol. 113, pp. 9901 2000.
- [15] C. T. Sah, R. N. Noyce, and W. Shockley. *Proceedings of the IRE* 45, 9, pp. 1228 43, 1957.
- [16] W. Shockley and W.T. Read, "Statistic of the Recombinations of Holes and Electrons," *Phys. Rev.*, vol. 87, pp. 835, 1952.
- [17] C. Virmontois « Analyse des effets des déplacements atomiques induits par l'environnement radiatif spatial sur la conception des imageurs CMOS ». Toulouse, *PhD thesis*, ISAE, 2012 available on [http://depozit.isae.fr/theses/2012/2012\\_Virmontois\\_Cedric.pdf](http://depozit.isae.fr/theses/2012/2012_Virmontois_Cedric.pdf)
- [18] J. M. Belloir, V. Goiffon, C. Virmontois, P. Paillet, M. Raine, R. Molina, C. Durmez, O. Gilard, P. Magnan, "Dark current spectroscopy on alpha irradiated pinned photodiode CMOS image sensors," *IEEE Trans. Nuc. Sci.*, vol 63(4), pp. 2183-2192, 2016.



- 
- [19] S.J. Watts, J. Matheson, I.H. Hopkins-Bond, A. Holmes-Siedle, A. Mohammadzadeh, R. Pace, "A new model for generation-recombination in silicon depletion regions after neutron irradiation," *IEEE Trans. Nucl. Sci.* vol 43, pp. 2587-2594, 1997.
- [20] J.M. Belloir, "Spectroscopie du courant d'obscurité induit par les effets de déplacement atomique des radiations spatiales et nucléaires dans les capteurs d'image CMOS à photodiode pincée", Toulouse, PhD Thesis, ISAE, 2016.
- [21] L.C. Kimerling, "Radiation Effects in Semiconductors", *Conf. Ser.* vol. 31, pp. 221, 1977.
- [22] P. Vadja, and L.J. Cheng, "Low temperature photoconductivity in electron-irradiated p-type Si", *J. Appl. Phys.* vol. 42, pp. 2453, 1971.
- [23] J. Bourgoin and M. Lannoo, "Point Defects in Semiconductors II, Experimental Aspects," *Sol. Stat. Sc.*, vol. 35, 1983.